Journal of Power Sources 183 (2008) 260–274

Contents lists available at ScienceDirect

Journal of Power Sources

journal homepage: www.elsevier.com/locate/jpowsour

Review

A review on PEM voltage degradation associated with water management: Impacts, influent factors and characterization

N. Yousfi-Steiner[a,b], Ph. Moçotéguy[a,*], D. Candusso[c,b], D. Hissel[b], A. Hernandez[b], A. Aslanides[a]

[a] EIFER, European Institute for Energy Research, Emmy-Nother Strasse 11, 76131 Karlsruhe, Germany
[b] FEMTO-ST/ENISYS FCLAB, UMR CNRS 6174, University of Franche-Comté, rue Mieg, 90010 Belfort Cedex, France
[c] INRETS, The French National Institute for Transport and Safety Research, 2 avenue du Général Malleret-Joinville, 94 114, ARCUEIL Cedex, France

ARTICLE INFO

Article history:
Received 19 February 2008
Received in revised form 31 March 2008
Accepted 9 April 2008
Available online 22 April 2008

Keywords:
PEM fuel cell
Water management
Characterization technique
Fault tree
Flooding
Membrane drying

ABSTRACT

Water management is one of the most important issues in Proton Exchange Membrane Fuel Cells (PEMFC). Flooding and drying out are the two main degradation mechanisms that occur when water management is not adequate. This paper overviews the underlying phenomena linked to water management and some characterization methods or strategies to prevent their occurrence. Finally, a fault tree is built, in order to discriminate the different defaults and better understand the relationship between the causes and symptoms.

Contents

* Corresponding author. Tel.: +49 721 610 513 37; fax: +49 721 610 513 32.
E-mail addresses: nadia.steiner@eifer.org (N. Yousfi-Steiner), philippe.mocoteguy@eifer.org (Ph. Moçotéguy), denis.candusso@inrets.fr (D. Candusso), daniel.hissel@univ-fcomte.fr (D. Hissel), andres-ignacio.hernandez@utbm.fr (A. Hernandez), antoine.aslanides@eifer.org (A. Aslanides).

0378-7753/$ – see front matter © 2008 Elsevier B.V. All rights reserved.
doi:10.1016/j.jpowsour.2008.04.037

Nomenclature

d_h	hydraulic diameter (m)
$D_{(.)}$	diffusion coefficient ($cm^2\ s^{-1}$)
F	Faraday constant, 96.487 ($C\ mol^{-1}$)
g	acceleration of the gravity ($m\ s^{-2}$)
h_{fg}	latent heat of vaporization of water, 2260 ($kJ\ kg^{-1}$)
I	current density ($A\ cm^{-2}$)
K	permeability (m^2)
k_c	rate constant for condensation (s^{-1})
M	molar mass ($kg\ mol^{-1}$)
n	moles number (mol)
P	pressure (Pa)
Q	volumetric flow rate ($m^3\ s^{-1}$)
R	gas constant, 8.314472 ($J\ mol^{-1}\ K^{-1}$)
s	volume fraction occupied by liquid water
S	surface area (m^2)
t	time (s)
T	temperature (K)
v	velocity ($m\ s^{-1}$)
V	volume (m^3)

Greek letters

ε	electrode porosity
ϕ	relative humidity
λ	membrane water content
μ	kinematic viscosity ($m^2\ s^{-1}$ or Pa s)
ρ	volumetric mass ($kg\ m^{-3}$)

Subscript, superscript

a	anode
acc	accumulation
c	cathode
cond	condensation
ev	evaporation
ext	external
g	gas
H_2O	relative to water
in	inlet
l	liquid
m	membrane
o	dry
out	outlet
prod	production
sat	saturation
T	total
v	vapour
(.)	relative to anode or cathode

1. Introduction

Polymer Electrolyte Membrane Fuel Cells (PEMFC) convert directly the reactants' chemical energy into electrical energy with high efficiency, high power density, and good environmental compatibility [1]. This explains why its development draws more and more attention. Among the various stakes associated with fuel cells development, reliability, cost and durability appear to be the most important considerations to successfully achieve its commercialization. Indeed, to be able to compete with conventional combustion engines, the minimum lifetime requirements are 40,000 h for stationary applications and varies between 5000 and 20,000 h for automotive applications. At first sight, due to the absence of moving parts, fuel cells would appear to be inherently more reliable than conventional combustion engines. However, they are prone to material degradation and their internal components are placed under mechanical constraints. A huge effort is thus made worldwide to understand the degradation mechanisms so as to increase their lifetime.

Several studies [2–14] have shown that the lifetime of a PEMFC can be reduced by several factors such as membrane degradation, catalyst dissolution and agglomeration. Lifetime can be reduced due to either long-term operation (power or thermal cycling) or to operation incidents such as reactants starvation or MEA contamination. A complete overview of issues associated with chemical contamination in PEMFC has recently been performed by Cheng et al. [3].

In this paper, we will focus on the degradation that stems from an improper water management: namely drying out and flooding which issues have been reviewed in a very recent work by Liu and co-workers [4]. The authors have discussed the effect of flooding on the cell performance, but also the contribution of cell design and material in this issue, therefore, it will not be the purpose of this paper. Our work aims at bringing the light on the consequences of a non-equilibrated water balance which leads to flooding or drying out as extreme consequences. It reviews in detail the influence of operating conditions and parameters that have a great impact in this disequilibrium and tries, through a water balance equation to analyze the contribution of each factor. To provide a better insight into the PEM degradations associated with water management, a fault tree is built, revealing the connections between causes and symptoms. This analysis helps in defining simple characterization methods for these failures using a minimum of additional sensors, which is the most suitable diagnostic system in a real transportation application. Thus, even if several usual characterization methods able to detect and discriminate the various degradation modes will be listed, we will mainly focus on non-intrusive *in situ* ones. These are easy to implement, reproducible on a large set of fuel cell designs and are able to deliver an optimum set of information about the evolution of the parameters (membrane resistance, . . .) during the fuel cell operation.

2. Polarization losses

A PEMFC consists of two electrodes in contact with a membrane separating gas compartments. The electrodes are constituted by a gas diffusion layer (GDL) and an active layer (AL), which both have a porous structure. This assembly is sandwiched between two current collectors, also known as bipolar plates, in which gas dis-

tribution channels are integrated. The active layer consists mainly of catalyst particles, ionomer and pore spaces which form a three-phase boundary where electrons, protons and reactant gases meet and where the electrochemical reaction takes place.

Fuel cell degradation results in the decrease of its voltage and power output, either due to a long-term ageing or to a detrimental operating conditions. The fuel cell voltage under current flow is given by the following relation:

$$V = V_{eq} - \eta_{activation} - \eta_{concentration} - iR \quad (1)$$

where V is the cell voltage, E_{eq} the cell voltage at zero current also called open circuit voltage (OCV), η_x are the activation and concentration polarizations and iR is the ohmic drop.

OCV theoretically corresponds to the difference between the equilibrium potentials (i.e. Nernst potentials) of oxygen reduction reaction (ORR) and hydrogen oxidation reaction (HOR). Its value is 1.23 V at standard conditions (namely, temperature of 273.15 K (25 °C), all gases partial pressure of 10^5 Pa (1 bar) and protons concentration of 1 M). However, under fuel cells operational conditions, the real value is about 1 V [5].

$$V_{eq} = E_{eq.O_2/H_2O} - E_{eq.H^+/H_2} \quad (2)$$

During fuel cell operation, OCV deviates from its theoretical value basically because of reactants partial pressure drop associated with permeation through the membrane (H_2 crossover from the anode to the cathode) [6,7]. Possibly also from the reactions between Pt surface and O_2 or impurity oxidation [5] resulting in a mixed cathode potential [8]. Moreover, the activation polarization corresponds to performance losses due to the slowness of electron-transfer reactions at both electrodes and can be defined as:

$$\eta_{activation} = \eta^c_{activation} + \eta^a_{activation} \quad (3)$$

Activation polarizations appear already at low current densities. The $\eta^c_{activation}$ represents the major part of these losses because the oxygen reduction reaction at the cathode is several orders of magnitude slower than the hydrogen oxidation reaction [9]. The activation losses increase as the catalyst (contamination by reformate, dissolution and obstruction) or the ionomer which is in contact with it (dissolution, contamination) degrades. The mass transport losses or concentration losses reflect the mass transfer limitations associated with the reactant gases diffusion from the supply channels to the sites where electrochemical reactions take place. This can be expressed as:

$$\eta_{concentration} = \eta^c_{concentration} + \eta^a_{concentration} \quad (4)$$

The concentration losses are predominant at high current densities when the fuel cell is operating in conventional conditions (T, gas feeding). They are also usually linked with an improper water management, an insufficient reactants feeding or a GDL contamination.

The ohmic drop originates from the resistance of the entire cell component to the charge transfer (both electrons and protons) [14]. The ohmic losses are intrinsic to the cell, their increase being related to several possible mechanisms like membrane drying [53], membrane contamination [3], high contact resistance cell elements, thermal degradations [10] (cycles of swelling and shrinkage, frost) or metallic bipolar plates corrosion.

A typical evolution of fuel cell voltage with applied current is represented in Fig. 1. In this figure-type, V_{eq}(th) is the theoretical OCV previously described, and the V_{eq} is the OCV actually measured. This so-called polarization curve or I–V curve characterizes the overall stationary performance of either stacks or single cells [11]. Three different regions (I, II and III) can be distinguished in this curve, each one being associated to specific degradation mechanism. The first one, for low current densities, is associated with activation losses and possibly fuel crossover through the membrane, oxidation of the platinum, carbon or other impurities as well as internal short circuit [12]. In the second part, at medium current densities, the losses due to ohmic resistance are added to the activation losses and represent the major part of voltage losses. In the last part, the concentration polarization effect combines with the two previous effects and becomes the main contributor to the voltage losses. Performance of a fuel cell is usually expressed either in term of output current density at fixed potential or in term of potential at given applied current.

3. Water management issues in PEM fuel cells

The operation of PEMFC is fundamentally linked with the presence of water molecules in the cell. Water management has a major impact on the PEMFC performance, stability and lifetime, as reported in [13,14].

3.1. Water management issues

During normal PEMFC operation, water is produced by the ORR. As a consequence, its concentration at the cathode side is higher than at the anode side. Water thus diffuses from the cathode to the anode so as to equilibrate the concentrations between the two compartments. This phenomena is widely known as diffusion [15] or back-diffusion. However, in an aqueous medium, protons are surrounded by a certain amount of water molecules that constitute their solvatation shell. Drawn by the electric field, protons migrate from the anode to the cathode, dragging these water molecules. This phenomenon is widely known as electro-osmosis drag [14,15]. Zawodzinsky et al. [16] measured the electro-osmotic drag at 30 °C, by applying current through a Nafion 117 membrane separating two compartments and by monitoring the change in the height of water contained in capillary columns connected to the compartments. The authors measured a drag coefficient between 2.5 and 2.9 H_2O/H^+ for a membrane immersed in liquid water (conditions at which membrane hydration λ is maximal and equals 22) and 0.9 H_2O/H^+ when the membrane is in equilibrium with water vapour (conditions at which $\lambda = 14$) (Eq. (5)).

The relation given by Karnic et al. [17] is

$$n_{drag} = 0.0029\lambda_m^2 + 0.05\lambda_m - 3.4 \times 10^{-19} \quad (5)$$

Eq. (5) fits the previously mentioned experimental results. At low current densities, back diffusion will prevail on electro-osmosis, while for high current densities, electro-osmosis will prevail on back diffusion and the anode will tend to dry out, even if the cathode is well hydrated [18,19].

On one hand, water is needed to guarantee good proton conductivity in the ionomeric phase of both membrane and active layers, by dissociating the sulfonic acid bond [20]. Protonic conductivity is maximal in wet conditions because protons move in the hydrated parts of the ionomer, where the sulfonic acid bond can be dissociated, mainly by "jumping" from an acid group to another [19]. As a consequence, in a dry ionomer phase, where the sulfonic acid bond cannot be dissociated, the protons cannot migrate and the conductivity is decreased. A fully hydrated membrane has thus been proved to exhibit up to 300 times higher conductivity than a dry one [19,76]. In addition, a low ionic conductivity hinders the access of protons to the catalyst surface, decreasing the actual number of possible reacting sites in the three-phase boundary layer, thus increasing the activation polarization [21]. In term of localization, the drying out preferentially takes place at the anode side because the electro osmotic drag is usually higher than the back diffusion,

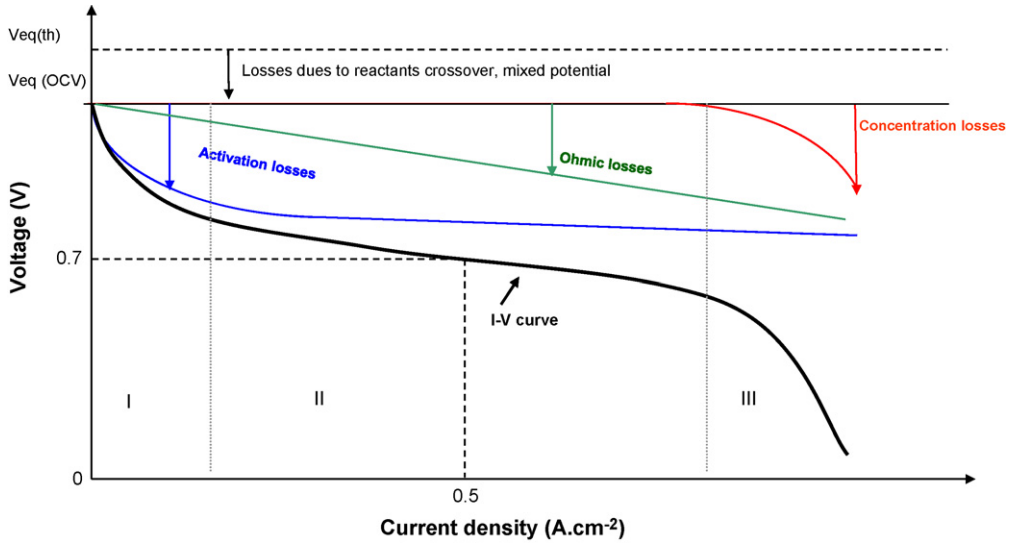

Fig. 1. Aspect of the polarization curve with the different voltages losses.

especially for high current densities and also because water is produced at the cathode side [22]. Finally, severe drying conditions have been proved to lead to irreversible membrane degradations (delamination, pinholes) within about 100 s [23,24].

On the other hand, the presence and accumulation of liquid water in the flow-field channels and/or electrodes gas porosities causes flooding, that hinders gas diffusion [25]. Natarajan and Nguyen [32] characterized, using a segmented electrodes cell, the flooding behaviour under potentiostatic conditions. They observed that flooding induced a heterogeneous output current distribution along the gas channels with a lower output current density closed to gas channels outlet. Flooding was characterized by sharp stepwise drops in the local current densities that they linked to the wettability and pore size distribution through the electrode. They hypothesize that the stepwise drops in the current density represent the filling up of the pores. When some parts of the electrodes, mostly closed to gas channel outlet, operated in conditions such that the major part of the pores were filled with liquid water, they measured a local output current density close to 0. At this stage, it is interesting to point out that such heterogeneities of current distribution observed in a small laboratory scale fuel cell (9 cm of gas channel length between extreme operating segment edges with 1 cm^2 active area) should be enhanced in a bigger surface cell.

At stack level and particularly at low gas stoichiometries, cells are fed with gas in parallel and gas flow is unevenly distributed due to differences in each cell's resistance to gas flow, either associated with flow field design, electrode material or accumulation of liquid water. As a consequence, as the stacks operate in galvanostatic mode, the current distribution heterogeneities observed by Natarajan and Nguyen at single cell level [32] manifest themselves in a heterogeneous cell voltages distribution within the stack [5,67], because of uneven distribution of impedance associated with gas diffusion to reacting sites. Thus, Rodatz et al. [5] compared the individual cell voltage distribution for three different applied current density levels (low, medium and high). They observed that, for the low current densities, the standard deviation of the cell voltage is small, indicating a quite homogeneous cell voltage distribution. This value increases with the current, reaching a value of 5% or more for high current density (100 cells at 70 A).

Fouquet et al. [26] found that a cell flooding occurs in two steps: first, water droplets build-up while cell voltage drops quite slowly; and, after several minutes, the droplets aggregate and block the gas channels, impeding reactants diffusion to the catalyst sites and inducing in turn a rapid cell voltage drop. Indeed, He et al. [27] experimentally proved, by following the pressure drop evolution in the cathode channel during the polarization curve measurement that the mass transfer limitation at high current densities is associated with flooding, as shown by a homogeneous fast increase of pressure drop in the cathode compartment.

Even if flooding generally occurs during operation at high current densities, several studies indicated that liquid water accumulation can be an issue in all operating regimes, particularly under low gas flow rates/temperature levels [28] or if liquid water is not properly removed from the channels [29,30]. Moreover, even if liquid water can flood at both electrodes [31,32], it is especially crucial at the cathode catalyst layer where it is produced by the ORR [33]. In addition, the localization of the flooding inside the electrode is difficult (channel/electrode or both). Natarajan and Nguyen [32] affirmed that the accumulation of the liquid water in the channels will be observed only after the complete saturation of the gas with water vapour since the evaporation and water vapour transport are relatively faster than liquid water transport (either by capillary mechanism within the GDL or, thanks to the drag force exerted by the convective flow of the gas in the vicinity of the channels). Similarly, Yamada et al. [34] affirm that the flooding in the AL and the GDL likely occurs prior to that in the gas channels, because the water is produced in the AL and then expelled through the GDL to the flow channels. But at low current densities, channels flooding is likely to occur without AL or GDL flooding, if inlet gases humidities are high and/or if cell temperature is low [35]. Once the channels flood, the evacuation of liquid water from the electrode is decreased because of the water evacuation towards the channels decreases due to the water saturation gradient decrease [32].

St-Pierre et al. [36] have shown that most of the consequences of a short-term flooding are reversible but also that a long-term operation under excess liquid water may lead both to mechanical degradation of the MEA's material and to local oxidant starvation.

As a consequence, a subtle equilibrium has to be found between membrane drying and liquid water flooding to prevent fuel cell degradation and guarantee a high performance level. Larminie and Dicks [14] recommended that humidity of the air should be above

80% to prevent excess drying and below 100% (gases contain liquid water droplets) to avoid liquid water in the electrodes/gas channels.

As insight to the water management issue, one can analyze the fuel cell water molar balance, as function of the operating parameters: current density, inlet gases flow rates and relative humidity, fuel cell temperature. The water vapour partial pressure is associated with the two latter parameters through the saturation pressure of water, which evolution follows an exponential trend versus temperature according to the Clapeyron relation [37] applied between a saturated state and an known state:

$$P_{\text{sat}} = P_0 \mathrm{e}^{-(M_{\mathrm{H_2O}} h_{\text{fg}}/R)(1/T - 1/T_0)} \tag{6}$$

where P_0 is the pressure at the known temperature T_0, $M_{\mathrm{H_2O}}$ the molar mass of water (kg mol^{-1}), h_{fg} the water latent heat of vaporization (kJ kg^{-1}), R the gas constant (J mol^{-1} K^{-1}), T the temperature (K) and T_0 is a known temperature (K).

In a simplified approach, the cell is divided in three different elements electrode/membrane/electrode as shown in Fig. 2. For each domain, the molar flow rates of entering, leaving and produced water are taken into account, either in liquid or vapour phase. In each domain, the variables such as temperature, humidity ratio, gas flow rates, total gas pressure, volume fraction of liquid water are considered as homogeneous.

According to this approach, water molar balance in cathode, anode and membrane can, respectively, be written as follow:

$$\left(\frac{\mathrm{d}n_{\mathrm{H_2O}}}{\mathrm{d}t}\right)_{\text{acc,c}} = \left(\frac{\mathrm{d}n_{\mathrm{H_2O}}}{\mathrm{d}t}\right)_{\text{in,c}} - \left(\frac{\mathrm{d}n_{\mathrm{H_2O}}}{\mathrm{d}t}\right)_{\text{out,c}} + \left(\frac{\mathrm{d}n_{\mathrm{H_2O}}}{\mathrm{d}t}\right)_{\text{prod,c}} - \left(\frac{\mathrm{d}n_{\mathrm{H_2O}}}{\mathrm{d}t}\right)_{\text{c}\to\text{m}} \tag{7}$$

$$\left(\frac{\mathrm{d}n_{\mathrm{H_2O}}}{\mathrm{d}t}\right)_{\text{acc,a}} = \left(\frac{\mathrm{d}n_{\mathrm{H_2O}}}{\mathrm{d}t}\right)_{\text{in,a}} - \left(\frac{\mathrm{d}n_{\mathrm{H_2O}}}{\mathrm{d}t}\right)_{\text{out,a}} - \left(\frac{\mathrm{d}n_{\mathrm{H_2O}}}{\mathrm{d}t}\right)_{\text{a}\to\text{m}} \tag{8}$$

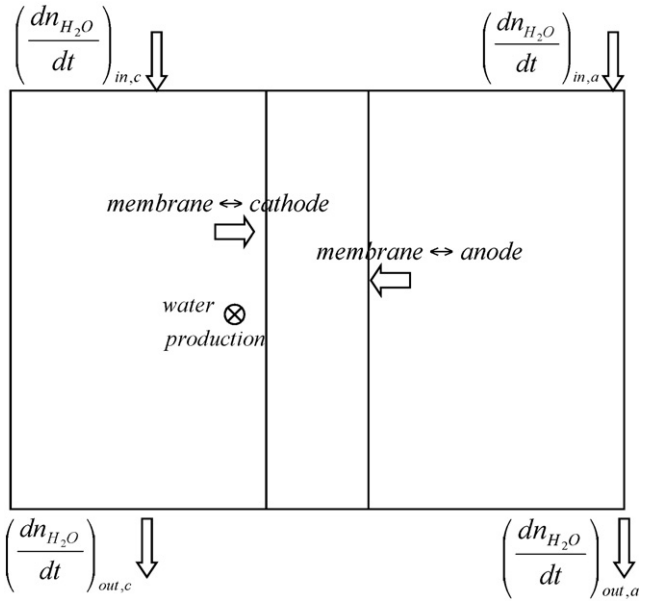

Fig. 2. Water transfers in the cell.

$$\left(\frac{\mathrm{d}n_{\mathrm{H_2O}}}{\mathrm{d}t}\right)_{\text{acc,m}} = \left(\frac{\mathrm{d}n_{\mathrm{H_2O}}}{\mathrm{d}t}\right)_{\text{c}\to\text{m}} + \left(\frac{\mathrm{d}n_{\mathrm{H_2O}}}{\mathrm{d}t}\right)_{\text{a}\to\text{m}} = N_{\mathrm{SO_3}} \frac{\mathrm{d}\lambda}{\mathrm{d}t} = C_{\mathrm{SO_3}} V_{\text{m}} \frac{\mathrm{d}\lambda}{\mathrm{d}t} \tag{9}$$

where $(\mathrm{d}n_{\mathrm{H_2O}}/\mathrm{d}t)_{\text{acc}}$ is the water molar flow rate accumulated either in the electrodes or the membrane.

It is worth mentioning that the molar flow rate of water at each compartment/membrane interface corresponds to the net molar flow rate of diffusion and electro-osmosis at each interface. In the present case, we implicitly assume that the water molar flow rate on the compartment side of the interface strictly equals the one at the membrane side of the interface, which in turn implies that the water equilibrium at both interfaces are instantaneous.

Each term contribution is described and analyzed in Appendix A. From this analysis, the water molar balance in the whole cell can be written as follow:

$$\begin{aligned} &C_{\mathrm{SO_3}} V_{\text{m}} \frac{\mathrm{d}\lambda}{\mathrm{d}t} + \left(\frac{\rho_{\mathrm{H_2O,l}}}{M_{\mathrm{H_2O}}} - \frac{P' \mathrm{e}^{-(M_{\mathrm{H_2O}} h_{\text{fg}}/RT)}}{RT}\right)\left(V_{\text{T,a}} \frac{\mathrm{d}s_{\text{a}}}{\mathrm{d}t} + V_{\text{T,c}} \frac{\mathrm{d}s_{\text{c}}}{\mathrm{d}t}\right) \\ &= -\frac{P' \mathrm{e}^{-(M_{\mathrm{H_2O}} h_{\text{fg}}/RT)}}{RT}\left[\frac{\mathrm{d}V_{\text{a}}}{\mathrm{d}t}(1-\phi_{\text{a,in}}) + \frac{\mathrm{d}V_{\text{c}}}{\mathrm{d}t}(1-\phi_{\text{c,in}})\right] \\ &\quad + \frac{I}{2F} - \frac{\rho_{\mathrm{H_2O,l}}}{M_{\mathrm{H_2O}}} \frac{K_{\text{l}}}{\mu_{\text{l}}}\left[s_{\text{a}}\left(\frac{K_0}{K_{\text{g}}}(1-s_{\text{a}}) - 1\right)(P_{\text{a}} - P_{\text{ext}})\right. \\ &\quad \left. + s_{\text{c}}\left(\frac{K_0}{K_{\text{g}}}(1-s_{\text{c}}) - 1\right)(P_{\text{c}} - P_{\text{ext}})\right] \end{aligned} \tag{10}$$

The first and second terms in the left side of Eq. (10) represent, respectively, the variation of the amount of water in the membrane and in each compartment (in liquid form). If these terms are positive, then membrane hydration and liquid water formation will, respectively, be favoured. Oppositely, if they are negative, membrane drying will be favoured and liquid water formation will be prevented.

As a consequence, it appears from equation (Eq. (10)) that any increase in gas inlet flow rate or any decrease in gas inlet relative humidity will impact negatively the left side term.

Similarly, since $\rho_{\mathrm{H_2O,l}}/M_{\mathrm{H_2O}} \gg P' \mathrm{e}^{-(M_{\mathrm{H_2O}} h_{\text{fg}}/RT)}/RT$ even at 100 °C, any increase in temperature will also impact negatively the left side term. Such variations of parameters will consequently favour membrane drying and prevent water flooding. An opposite variation of these parameters will in turn prevent membrane drying and favour compartment flooding with liquid water.

Interestingly, in absence of liquid water, the second term in the left side of equation (Eq. (10)) is zero, and so is the last term in the right side. This implies that, in this case, a variation of any operating parameter will directly and only impact the membrane water content.

However, we need to point out that, as described above, liquid water can be present in the cathode compartment while being absent from anode compartment. In this case, water management is even trickier because one would aim to simultaneously avoid membrane drying from the anode side and water flooding at the cathode side. This needs for water to be brought from cathode to anode, but as not shown by our simplified analysis, this transfer is not instantaneous. Indeed, the transient of liquid water response has been proved to be in a time scale of about 20 min [26]. Even if we are aware that the considerations of our model are very rough, we think that they are sufficient for an overall analysis of water mass balance issue. A complete and detailed analysis of water mass balance issue is beyond the scope of this paper.

Therefore, a proper water management consists of maintaining, during fuel cell operation, the fragile equilibrium between:

- The water carried inside and outside the cell by the inlet and outlet gases.
- The water generated in the cathode catalyst layer by the electrochemical reaction.
- The water transported by electro-osmosis and back diffusion.

This explains why stable performance (which means an equilibrated water balance) is achieved in a relatively narrow operational conditions window [38].

3.2. Water management strategies

In order to prevent the fuel cell from the damages associated with bad water management, several authors paid attention in defining efficient water management strategies. Strategies such as pressure drop, temperature gradients and counter-flow operation are easy to implement and have been found to reduce mass transport limitations associated with limited water management, especially at high current densities and low oxidant stoichiometries (the ratio between the quantity of inlet reactant to the one exactly needed for the electrochemical reaction) [39].

3.2.1. Controlling reactant humidity

Usually, the inlet gases are humidified prior to their access to the cell [14]. However, some authors demonstrated that fuel cells could also operate without inlet humidification at the cathode and/or the anode side [40,41]. In this case, an optimum set of parameters (flow rate, cell area, current density, temperature, type of the membrane) must be chosen carefully to use the produced water for cell hydration and achieve effective inner humidification. This operating mode is known as "internal humidification mode" [18].

In this case, when the dry gases come in contact with the ionomer electrolyte, part of the water it contains evaporates, humidifying the gases and drying the ionomer. To guarantee a successful operation without inlet humidification, the amount of water required to saturate the reactant gases must be lower than the amount of water generated by the ORR. Since the presence of liquid water is very unlikely in absence of gas humidification, this means that, the sum of the two first terms at the right side of equation (Eq. (10)) must be positive. Buechi and Srinivasan [41] observed that the cell performance is 40% lower when operated without humidification compared to operation with humidified gases conditions. The authors explained this performance loss by lower water content or a steep water concentration gradient in the membrane.

Referring to the simplified model presented before (Eq. (10)) an operation with "internal humidification mode" implies to decrease the operating temperature so as to limit the amount of water that could evaporate and go out of the cell with the exhaust gases. In practice, the cell temperature must not exceed 60 °C to avoid the risk of fierce drying by the gases [14,41].

As said before, the liquid water removal from the cathode is due either to evaporation or to water transport through the membrane towards the anode (back-diffusion) or water transport towards the channel for evacuation. The back-diffusion is influenced by many factors such as the humidification level of the anode gas stream. In their experiments with a segmented electrodes cell operating in potentiostatic (constant voltage) mode, Natarajan and Nguyen [32] showed that increasing the humidity level of inlet gas at the anode decreased the amount of liquid water transferred from the cathode to the anode by back-diffusion, leading to an increase in current distribution heterogeneities and a sooner appearance of liquid water which also impacted an increased number of segments.

Dehumidifying one or both reactant streams is also a corrective action which is used after cell flooding and which would promote water vaporization in the flow fields [36,42].

3.2.2. Controlling reactants flow rate

As previously described and according to equation (Eq. (10)), a lower flow rate will contribute to maintain water inside a drying cell but will favour flooding, which in turn might lead reactant depletion. To prevent this, the reactants will be actually fed to the cell at a higher rate than the one exactly needed for the electrochemical reaction. The stoichiometric ratio will be, in practice, higher than 2 for air [14]. A value of 1 for this ratio set the lowest limit for reactant flow rate control.

Natarajan and Nguyen [32] showed in their segmented electrodes cell and in potentiostatic mode that the liquid water movement inside the cell is a strong function of the gas velocity. Lowering the oxidant flow rate causes evaporation and liquid water removal by drag to be reduced. In this case, the inlet gases saturation occurs more quickly and is achieved closer to the inlet [32]. Consequently, a decrease in reactant flow rates induced an increase in current distribution heterogeneities. They also observed that an increased number of segments was affected by output current drop and that this drop occurred sooner. Oppositely, an increase in gas flow rates delayed the current drops associated with flooding in the segments closed to the gas channel outlet but induces a slight decrease of current density output in the segments closed to the gas channels inlet. They explained these results by a dryer membrane in the segment closed to the gas channel inlet inducing in turn a higher ohmic resistance. In their experiments, Hakenjos et al. [43] observed that when increasing reactant flow rate, an improvement of cell performance (higher output current density) due to the higher stoichiometry and the flush of the water out of the flooded cell. They also observed a rise of cell temperature in areas where liquid water is observed and attributed it to the enthalpy of condensing water.

Obviously, the impact of gas flow management on the stack lifetime should be evaluated. The work of Wahdame et al. [44] investigated the importance of gas flow management strategies, and observed that fuel cell durability is supposed to be strongly linked to the adopted strategy: for instance, mechanical stress can appear due to the pressure drops and hot spots can appear due to uneven flow and water distribution.

3.2.3. Controlling temperature

According to equation (Eq. (6)), increasing the operating temperature increases the saturation pressure and in turn the evaporation rate [27]. As a consequence, as shown by equation (Eq. (10)), the amount of liquid water in the cell is diminished and the effect of flooding mitigated [36]. In addition, He et al. [27] explained that surface tension and viscosity of liquid water decrease as temperature increases, which facilitates the flush of liquid water out of the cell. He et al. [27] thus observed a recovery of the flooded cell after applying a quick cell temperature ramp from 40 to 50 °C while fixing the other parameters (air flow rate, cell voltage).

3.2.4. Controlling pressure

In normal operating conditions, with homogeneous pressure, electro-osmosis flow rate is usually higher than back diffusion flow rate. To counterbalance this effect, Wilkinson et al. [45] and Voss et al. [46] have set a pressure gradient between the cathode and the anode ($P_a < P_c$) and observed an improvement of cell performances. This "AWR: Anode Water Removal" setup enables the water produced at the cathode to be drawn by a concentration gradient toward the anode and to be evacuated in this very side, preventing cathode flooding. However, on a practical point of view, this method is better suited for large surface area fuel cells, since the cell specific design (channel manufacturing) becomes more difficult and expensive as cell area decreases. In addition, an important pressure gradient can cause some mechanical membrane degradation.

As a consequence, the anode-cathode pressure gap is practically limited to about 500 mbar.

In another study, Rodatz et al. [5] used of pressure pulses to assist the removal of water droplets in the flow channels. These pressure waves consist on supplying the gas in short time intervals with higher pressure than the operating pressure or to put the cell exit in a low pressure vessel creating low pressure pulses. The wave is followed by a temporary increase in the flow, which remove the water droplets out of the cell.

3.2.5. Convenient fuel cell design

The fuel cell design and particularly the channels design play a major role in the water management problems. With the conventional (parallel) flow field, the flooding mitigation is possible only through increasing the evaporation rate (increasing temperature or gas velocity) [32]. A design that diminishes, in addition, the PEMFC mass transport constraints is the interdigitated flow field design [47]. In this gas management mode, the flow channel design is a dead-end mode, forcing the gas to flow through the porous GDL and converting the reactants transport from a diffusion mechanism to a forced convection mechanism. The force resulted from the gas flow helps flushing any liquid water that otherwise may accumulate in the GDL. In [47], Nguyen compared experimentally fuel cells with interdigitated and parallel straight channel flow fields. The author showed that the interdigitated design leads to better performance than the conventional design. These results are in accordance with the experiments of Wood et al. [48] that showed that the interdigitated flow design could extend the PEMFC operable regime to higher current densities and consequently, a 50–100% increase in the fuel cell performance could be obtained. Indeed, the stream can handle a higher water production flow rate with the interdigitated flow fields than with the conventional ones. The performance improvement was partly explained by a more uniform reactant supply in the interdigitated design.

Liu et al. [30] compared the liquid water accumulation in three different types of cathode flows channels design (interdigitated, cascade and parallel flow channels). During the operation, the water flooding appears later in the interdigitated and cascade channels than in parallel channels, size of flooding areas being also reduced.

Finally, cell components are designed to optimize water evacuation at the cathode. For instance, a fuel cell GDL typically contains PTFE because of its hydrophobicity [49]. The performance losses associated with liquid water accumulation could be reduced by adding some hydrophobic particles in the GDL [50] or by locally increasing the electrode substrate porosity near the oxidant outlet, where the water accumulates. Solutions to reach this goal is to use some carbon clothes instead of carbon fibre paper near the oxidant outlet, or simply to insert grooves or holes in the carbon fibre paper in areas where water accumulation is the most acute [23].

The thicker the membrane is, the better its mechanical durability and its tolerance to stress and pressure gradients, but the higher is the ohmic resistance. Therefore, and especially at high current densities, the dominant electro-osmotic drag tends locally to reduce water content in the membrane and in the anodic AL, transporting it to the cathode where it promotes the flooding. This leads to higher ohmic losses due to local membrane drying out, to higher concentration losses due to the flooding and to an additional non-negligible, activation overpotential for the HOR, as most of the anodic catalyst sites become inactive due to the low proton mobility in this dried zone [51].

3.2.6. Modifying the current density

The water production is directly linked to current density, as reflected by the term $I/2F$ in equation (Eq. (10)). Thus, the temporarily reduction of the current being drawn from the stack mitigates the flooding because it reduces the rate at which water is electrochemically produced [42].

3.3. Fault tree analysis

Widely used in operating safety and reliability science, the fault tree analysis (FTA) [52] enables to clear out the different contributions. A fault or failure tree is a graphical representation of the relationship between an undesirable event (called a top event) and all its potential causes. It is a "top-down" approach starting with the top event (failure, malfunction, ...) and determining all the causes that can lead to it. The analysis proceeds by determining how this top event can be caused by individual or combined lower level failures or events. FTA is a formal methodology for determining the combinations of component level faults that could result in the occurrence of specific failures at a system level.

Water management issues are mainly caused by perturbation in the membrane water balance and liquid–vapour equilibrium. As shown by Eq. (10), a high temperature and high gas flow contribute to mitigate flooding by promoting dissolved water in the membrane and liquid water evaporation, causing possibly drying out of the membrane, while high current density means high water production that promote flooding just like low flow rate and relative humidity. Simplified fault trees have been built both for flooding and membrane drying out and are reported in Fig. 3(a) and (b). These fault trees do not take into account very specific cases in which the evolution of influent parameters can counteract to result in a non-straightforward variation of the event. For instance, in case of opposite variation of water production rate and water vapour inlet feeding, the sense of variation of water vapour partial pressure depends on their respective magnitude.

4. Experimental methods for the characterization of water management issues

Despite the good knowledge of the parameters that influence water equilibrium in the cell, a hurdle to its active control is the lack of adequate tools for monitoring fuel cell inner humidity level [53] and the difficulty in observing the flooding [34].

Characterization techniques allow a quantitative comparison of fuel cell systems, distinguishing effective fuel cell designs from poor ones. The best technique should discriminate between the various sources of loss within a fuel cell: activation, ohmic, mass transport loss [54].

An exhaustive list of experimental methods that allow an *in situ* water content monitoring can be found in the work of St-Pierre [55].

These techniques can characterize various fuel cell properties [54], like kinetic properties by assessing the electrochemical surface area (ESA), the activation polarization or the exchange current density. The ohmic properties are usually characterized by the determination of the ohmic resistance, the membrane ionic conductivity and other resistances (contact, electrode, bipolar and terminal plates' resistance). Finally, the mass transport properties could be characterized by determining diffusivity coefficients, pressure drop, limiting current density, ...

Numerous studies characterize overall performances before pointing out specific properties; the most common way is to build up the overall relationship between voltage and current or between power and current. Finally, for durability issues, other properties such as lifetime, mechanical structures (like thickness, porosity, catalyst load, particles sizes), as well as cycling or fatigue, can be characterized.

All these characterization methods can be classified in different types: intrusive, non-intrusive, *in situ* and *ex situ* methods. *In*

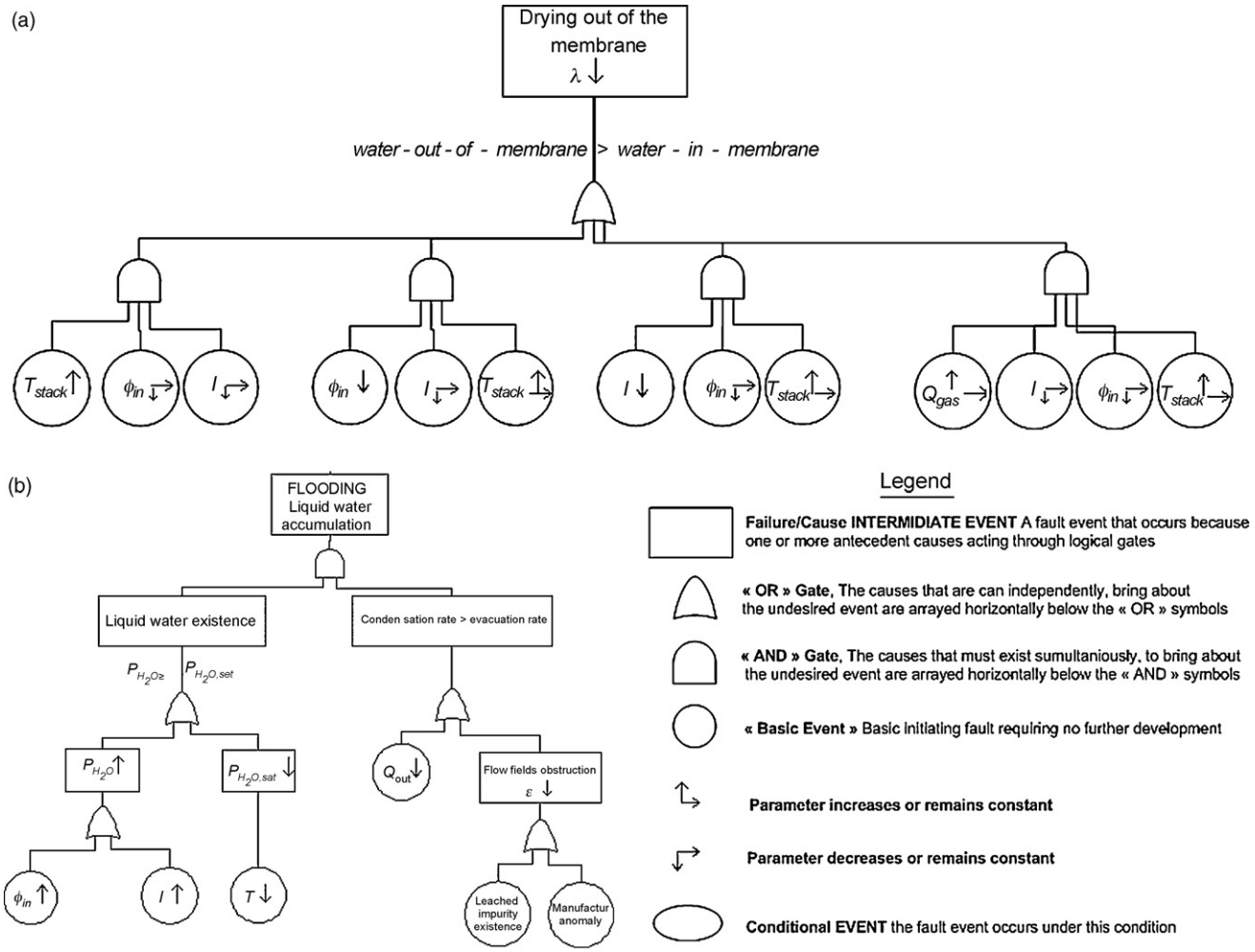

Fig. 3. (a) Root causes of the performance loss due to drying out and (b) root causes of the performance loss due to flooding.

situ methods are measurements that characterize the individual cell or the stack performance during its operation. Oppositely, *ex situ* methods refer to the methods that are not or cannot be used during fuel cell operation. We will define the intrusive methods as the measurements that use sensors in the cell, actions that can modify the fuel cell state (segmentation of the electrodes, for example) or methods that can only be implemented in a specific kind of fuel cell design, while the non-intrusive methods can be implemented in all fuel cells, and do not use inner sensors. Such kind of method is usually based on the cell response to given solicitations. The choice of the adequate method will depend on available information/data/resources, on which property we want to characterize and at which precision level.

Various experimental techniques have been employed to investigate the water dynamics in a PEM fuel cell [32,51–55,62,70–72].

Cell drying out is usually detected thanks to a membrane resistance increase [51–55]. Stumper et al. [21] used a so-called "Membrane Resistance and Electrode Diffusivity method" (MRED) which is an in situ method based on the galvanostatic cell-discharge with interrupted reactant supply and evacuation. This method provides information about flooding through the amount and the distribution of liquid water in the cell as well as the drying out of the cell through membrane water content. The ohmic cell resistance (thus, membrane water content) is deduced from the mass-transport-free transient polarization (voltages measured without concentration gradients). During cell discharge, the pressure and voltage decay give information on the effective diffusivity and the amount of liquid water present in the electrodes is deduced from the difference between the free gas volume in the dry cell and the free gas volume under given operating conditions.

Concerning flooding, several studies used the direct visualisation through transparent fuel cell [29,30,34,35,56,58], either in the GDL [34] or in the channels [29,30,56]. It results in reliable real-time detection of liquid water droplet formation and accumulation and allows the assessment of the influence of parameters such as cell temperature, current density and operating time [56].

Tueber et al. [56] investigated the effect of the wetting properties of the electrode on the flooding and thus on the cell performance. They showed that the use of standard, hydrophobized and hydrophilized carbon papers directly influence the accumulation of produced water in the gas channels of a transparent cathode. Hakenjos et al. [43] combined the visualisation through the cell with temperature and current distribution measurement through a segmented anode: when water is in the vapour phase, the high temperature regions correspond to higher currents. When the water is in liquid phase, the temperature increased in the flooded areas since the condensation of water releases heat. Thus, heat production adds up to an almost four-fold in the areas where water condensates when compared to the dry areas with the same current density.

On another hand, liquid water hinders gas transport and covers the active area which leads to a current density decrease in the flooded areas.

The two previous studies [43,56] were done at low temperatures (less than 37 °C) and low current density (maximum of 0.27 A cm^{-2}). Oppositely, Spernjak et al. [35] used the direct visualisation inside a cell in order to investigate the flooding under different GDL materials and under "realistic operation conditions": temperature around 80 °C and high water production rate; the maximal current density was around 2.6 A cm^{-2}.

Other imaging methods such as gas chromatography (GC) to measure the water vapour distribution in the flow channel [57], or neutron radiographic imaging that can detect the accumulation of liquid water in the flow fields and the GDL [25] have also been successfully used, even if sometimes constrainful. Less constraining methods like pressure drop monitoring [29–31,42,55,56,58], current voltage characteristics [59–61] and impedance techniques [13,26,62–64] will be detailed below.

This document will now focus on some non-intrusive *in situ* methods, reproducible on a large set of fuel cell designs and that can deliver an optimum set of information about the evolution of many parameters during fuel cell operation. Such methods are ideal to be used as simple diagnostic tools of the state-of-health of the fuel cell. They are summarized and compared in Table 1.

4.1. Polarization curve (I–V curve)

4.1.1. Polarization curve

As described in Section 2, fuel cell performance can be characterized by its polarization curve. Parameters such as OCV, cell polarization resistance, exchange current density, Tafel slope or limiting current may be approximated by comparing the analytical formulation of the polarization curve with experimental data [12,65]. Santarelli et al. [65] estimated the exchange current density, the polarization resistance and the internal current density (which is linked to the electrons and to the fuel crossing the membrane) with respective uncertainties of ±10%, ±1% and ±7%.

Comparison between polarization curves recorded in cell operated with air and pure oxygen is used to point out the mass transfer limitations located at the cathode side [23,36,66], possibly linked with water management (flooding). Ralph et al. [66] used air, helox (mixture of 79% helium and 21% oxygen, in which oxygen diffusion is easier than in air, thus reducing mass transport losses) and pure oxygen as oxidant. The performance losses between operation with air and helox are associated with oxygen gas diffusion while the performances losses between operation under helox and oxygen are associated with oxygen permeability losses. Using this technique, St-Pierre at al. [36] showed that a long-term exposure to excess water increases mass transfer losses.

Hernandez [67] affirmed that the influence of the liquid water on the cells performances is greater than the influence of gases pressures in the channels. Therefore, the dispersion of individual cell voltages was used as an indicator to characterize the flooding of the fuel cell.

4.1.2. Hysteresis (Fig. 4a and b)

Polarization curve is typically recorded by increasing the current from OCV until the limiting current (or at least a maximal current considered as relevant for a given application) is reached [68]. When it is recorded by increasing and decreasing the current density (upward and downward scan), the two resulting curves usually do not correspond in each point. This hysteresis can either indicate a flooding or a drying out of the cathode or of the anode. In fact, when a cell is flooding, the downward *I–V* curve would show lower voltages than upward *I–V* curve at high current densities (Fig. 4(b)). This is due to the increase of liquid water content in the electrode as additional water is produced by the growing current density. Conversely, if the cell is drying, production of additional water at high

Table 1
Comparison between characterization methods

Properties	CI method	HFR	AC resistance	EIS	Pressure drop
Invasiveness	In situ, time domain response Low: measurement equipment externally attached [55]; significant perturbation to the cell [10]	In situ, frequency domain response Low: minimal disturbance of the cell from its operating conditions [55,10]	In situ No electrochemical disturbance of the cell	In situ, frequency domain response Low: measurement equipment externally attached [55]; no electrochemical disturbance of the cell	In situ, time domain representation Low, Measurements performed outside of the cell [55]
Temporal	Sufficiently fast to capture several phenomena related to liquid water [55] (≈10 s)	Sufficiently fast to capture several phenomena related to liquid water [55] (≈10 s)		Sufficiently fast to capture several phenomena related to liquid water [55] (≈10 s)	Too slow to allow the capture of phenomena related to the liquid water [55] (≥10 s)
Reproducibility	≤5% of the average measured value	≤5% of the average measured value [55]		≤5% of the average measured value [55]	≤10% of the average measured value [55]
Error sources	Non-uniform current density distribution [10]; delay time [71]		Interference load/milliohm meter [10]		
Equipment	No need of additional equipment: the current interrupt can be performed by the load [71]	Frequency response analyzer [10]	Additional external frequency analysis equipment needed [10]	Frequency response analyzer [10] + electronic load + controller; impedance meter	External manometers
Miscellaneous	Suitable for high power systems [55] (residential vehicular fuel cell stacks)	Suitable for routine, periodic application during normal fuel cell operation results displayed in real time [10]		No [10]	
Can be conducted in parallel with the polarization curve?	Yes [10]			No [10]	
Quality of the results	Single data value easily interpreted [10]		Single data value easily interpreted [10]	Rich set of Data [10]; need to interpret the spectrum [10]	

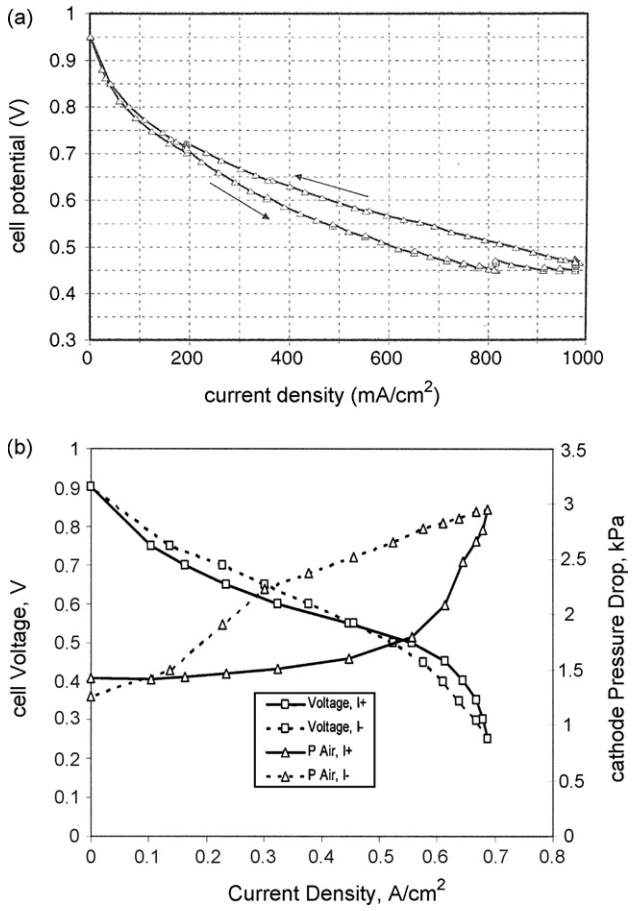

Fig. 4. (a) Hysteresis behaviour (polarization curve and pressure drop at the cathode) on drying cell [38] and (b) hysteresis behaviour (polarization curve and pressure drop at the cathode) on flooding cell [27].

current densities is "welcome" and would result in higher potential (Fig. 4(a)).

Note that the hysteresis can also be linked to the test protocol, namely current step duration, duration of the stabilization period, relative humidities, ...

In a general way, the polarization curve test is an interesting characterization method since it provides an indication of overall performance/degradation only by measuring current and voltage. However, it is not the preferred method to assess losses, since it does not provide sufficient information about key parameters that characterize fuel cell performances (membrane resistance, electrode diffusion, . . .) and do not give information about the time dependant processes that occur in the fuel cell, which are important for diagnosis purposes.

For example, for membrane resistance the discrepancies between the measured and the predicted values from the *I–V* curves could reach up to 45% [55]. This value grows with the long duration needed to achieve the curve recording [69]. For this purpose, other methods like current interrupt or impedance measurements (see below) are commonly used, usually in addition to the polarization curves.

4.2. Electrochemical impedance spectroscopy

The electrochemical impedance spectroscopy (EIS) is a dynamic characterization technique in which a small AC perturbation signal (voltage in potentiostatic mode, current in galvanostatic mode) is applied to the system, at various frequencies ranging typically from 10 kHz to 1 Hz. For each frequency, the magnitude and phase of the resulting signal (current or voltage) are measured and the impedance is determined.

EIS is widely used to characterize the water management in a fuel cell; as illustrated in [13,26] for flooding and [13,53] for drying out.

Le Canut et al. [13] showed that impedance spectroscopy was able to discriminate between a set of faults among drying, flooding and carbon monoxide poisoning. Fouquet et al. [26] coupled a model-based approach with electrochemical impedance spectroscopy measurements in order to identify parameters indicating flooding and drying.

The great advantage of the EIS method is the use of small signals that perturbs minimally the cell which nevertheless provides a rich data set from which many parameters could be extracted (electrolyte resistance, kinetic and mass transport polarizations within the fuel cell). The data result in spectra that allow interpretation [70]. Unfortunately, EIS is relatively time consuming [71], has a relative high cost [71] and is difficult to implement for high power fuel cell systems: theoretically, the polarization point is associated to (perfect/ideal) stable operating conditions which are rather difficult to obtain in the case of a high power stack.

4.3. Membrane resistance measurement

The electrolyte is the medium that ensures proton transport from one electrode to the other. The ohmic polarization comes from the resistance to ion transfer through the membrane and since this resistance depends on the operating conditions (temperature current density, hydration, . . .), it is imperative to determine it under these very operating conditions [10,70].

A direct method to measure the membrane resistance is to insert probes within it in order to define the voltage drop. This method is nevertheless highly invasive.

Three resistance measurements methods present a good compromise between simplicity, invasiveness and reliability: current interrupt (CI), AC resistance (ACR) and high frequency resistance (HFR). They all use the response of the cell to certain solicitations.

4.3.1. Current Interrupt method

This method consists in steeply interrupting the current while recording the voltage with a high acquisition rate. Since the potential change associated with the ohmic drop has a faster relaxation time than the relaxation times of electrochemical overpotentials, the two contributions can be easily isolated. This method measures the cell resistance during operation in the conditions prevailing just before the interruption. It is versatile, straightforward and fast. It can even be used for high power fuel cell system, either for determining the total ohmic losses in the stack or in each individual cell [72].

In an ideal way, the ohmic loss can be calculated from the difference between the voltage before and immediately after the current interruption. As a consequence, to get accurate results from the CI method, a well-adapted protocol and equipment is mandatory. Indeed, current must be sharply interrupted (within 0.01–0.1 ms) and a fast data acquisition system (>1000 samples s^{-1}) with high accuracy (around 1 mV for an individual cell voltage measurement) has to be employed to record the voltage response. A typical problem arising at low current densities is the inaccuracy of measured resistance when the *iR* value goes below the equipment's uncertainty limit [71]. Another critical situation arises when voltage measurement is not performed as close as possible to the fuel cell stack or individual cell connections. In this case and when long cables are used, the measured resistance is degraded because of

the "ringing effect" caused by the cable inductance, particularly for short delay times [10,38,71].

It is usual to implement a variation of this method in parallel with a polarization curve measurement by monitoring the voltage evolution associated with each current steps in order to determine the ohmic loss at the various *I–V* measurement points [54]. This way, "RI-free" or "RI-corrected" polarization curves can be built, and, when fitted to the Butler–Volmer equation, concentration losses can be separated from activation losses.

Mennola et al. [72] showed that current interrupt method could be used to isolate a poorly performing individual cell in a stack. At high air flow rates and high current density, they observed that cells in the centre of the stack exhibited ohmic losses up to 21% higher than the average value, probably because of a more severe dehydration in the middle of the stack. Abe et al. [64] investigated by the CI method the effect of oxygen relative humidity on the cell performance and showed that the decrease of cathode gas relative humidity induced an increase of total resistance. One third of this cell-resistance increase was attributed to the membrane and another third to the charge transfer resistance.

4.3.2. High frequency resistance (HFR) method

This method is actually a subset of the EIS method, since it has the same principle, but only a single frequency value is used (typically in the order of 1 kHz) and only the real component of the impedance is examined.

The optimal measurement frequency must be chosen with care [70]. This method disturbs minimally the cell from its operating conditions, both in magnitude and duration, and therefore it is suitable for routine, periodic application during normal fuel cell operation with a result displayed in real time [70].

General Motors has patented a method based on cell resistance monitoring for controlling the humidity level [73]. It correlated the fuel cell HFR to the degree of humidification in order to find the optimum humidification conditions. However, the HFR is not suitable to detect the cell flooding because flooding does not affect cell resistance.

4.3.3. High frequency milliohm meter (HFM) method or AC resistance method

In parallel to the load, an external AC milliohm meter is used to apply a fixed single frequency (typically in the order of 1 kHz) [34], in order to measure the total magnitude of both cell and load resistance in parallel. The resistance measurement is performed while the cell is in operation. The ohmic resistance of the electrolyte may be deduced after extracting the impedance of the load. Like EIS, this method perturbs minimally the cell. However, since the HF milliohm meter is installed in the same electrical circuit as the load, there may be some interference causing a considerable error in measurement.

4.4. Pressure drop

The frictions caused by the gas flow inside the electrodes and the channel result in a pressure drop between inlet and outlet channels. This parameter is very significant of the gases removal out of the cell.

The pressure drop along a flow field channel can be nicely described by the equation of the incompressible flow in pipes (Eq. (11)) as long as the pressure drop is less than 30% of the inlet pressure [38]:

$$\Delta P = f\frac{L}{d_h}\rho\frac{v^2}{2} + \sum K_L\rho\frac{\bar{v}^2}{2} \tag{11}$$

where ΔP is the pressure drop through the channel, f the friction coefficient that depends on many factors like the channel geometry, the shape of the cross-section, surface roughness, L the channel length (m), d_h the hydraulic diameter calculated as four times the channel cross-sectional area to its perimeter, $\bar{v}$ the average velocity ($m\,s^{-1}$) and K_L is the local resistance (sharp turns, change in the channel diameter, ...).

For the porous flow fields, as is the case for the GDL, the relationship between the pressure drop through the porous medium, the fluid viscosity and flow rate is given by the Darcy's law (Eq. (12)):

$$\Delta P = \mu\frac{Q}{AK}L \tag{12}$$

where ΔP is the pressure drop through the porous medium, Q the volumetric flow rate ($m^3\,s^{-1}$), K the permeability coefficient of the flow field (m^2), A the cross-sectional area (m^2), L the channel length (m) and μ is the cinematic viscosity (Pa s).

In the case of parallel flow field channels, the pressure drop along the channels corresponds to the pressure drop in the entire flow field [38].

For the interdigitated channels, since the gas entering the electrode is forced to flow through the porous backing layers to exit, the pressure drop between the inlet and the outlet of gases channel is mainly due to the forced gas flow through the porous GDL [27], in this case also, the pressure drop monitored between the inlet and outlet of the gas channels is mainly due to the pressure drop through the GDL.

In a general way, Darcy's law can be used for any flow field, as long as the flow is laminar, which remains valid, in most cases for flows through PEM fuel cells [38].

In case of two-phase flow in the channels, Rodatz et al. [5] reported that the pressure drop is calculated thanks to the following trapezoidal rule:

$$\Delta P = \int_0^L G^2(y)\left(\frac{2(yf(y)+K)v_g(y)}{d_h}\times\left(1+\frac{x(y)+v_{fg}(y)}{2v_g(y)}\right)\right)\mathrm{d}y \tag{13}$$

where G is the mass velocity, y the axial co-ordinate, v_g the specific volume of the gas phase, v_{fg} the difference in specific volume between the gas and liquid phases, d_h is the hydraulic diameter and x is the mass vapour quality [5].

Thus, according to Darcy law (Eq. (12)), for a given gas flow rate, the presence of liquid water reduces the cross-sectional area available for gas diffusion which in turn reduces the gas permeability K, and then, lead to an increase of the pressure drop. Thereby, the pressure drop in the flow fields varies as a function of the flooding level, and can indicate the liquid water presence. It increases as temperature decreases (condensation rate increases) and as current increases (increase in the amount of produced water). In addition, Rodatz et al. [5] affirmed that the compression of the cell could have an effect in improving the flooding and thus the pressure drop, since the GDL which is compressed between two flow channels, may intrude in these latters resulting in a smaller cross-area and therefore a greater friction factor.

The pressure drop is monitored by two pressure sensors located at gas inlet and outlet channels, or directly by a differential gas sensor. The use of this parameter as flooding characterization and diagnosis tool presents several advantages: it is non-intrusive, easy to implement and gives reasonably accurate results.

Generally, the pressure drop observed at the cathode side is higher than at the anode side. This is due to many reasons: the air flow rate is usually higher than hydrogen flow rate, the higher dynamic viscosity for air and oxygen than for hydrogen and/or most probably, the liquid water amount is higher in the cathode

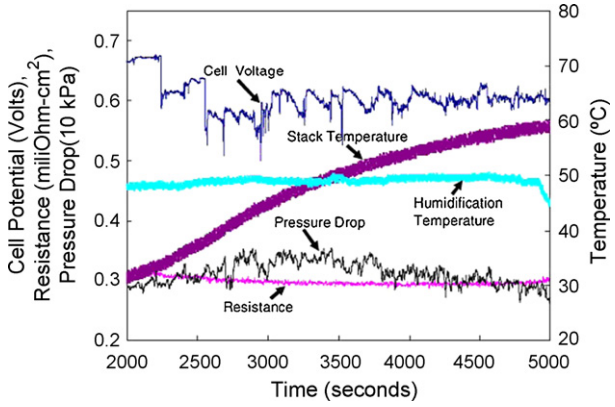

Fig. 5. Aspect of the three-cell stack voltage after flooding and recovery [31].

side (because of water production and possibly accumulation from previous operations).

Several studies used pressure drop measurement to investigate GDL or channels flooding [27,29–31,42]. He et al. [27] monitored the pressure drop at the cathode and showed a strong dependence between "flooding level" and the amplitude of the losses due to mass transfer limitations that they associated to cell flooding.

Liu et al. [30] have measured the pressure drop at both electrodes and studied the influence of operating parameters such as cell temperature, current density and operating time. They defined a parameter assessing the channel flooding rate as a function of the pressure drop.

General Motors patented a method and an apparatus for flooding detection [42] based on pressure drop monitoring and comparison to a threshold value beyond which corrective actions are triggered (humidification reduction, gas flow rates increase, gas pressure decrease and/or current reduction).

Unfortunately, pressure drop measurement is not sufficient to accurately localize the flooding inside the cell (AL, GDL or channel). To this aim, other techniques previously named such as visualisation techniques through a transparent fuel cell [29,30,34,35,43,56,58] and/or measurements of current and temperature distributions [43] have to be used.

Finally, the pressure drop can be influenced by the fuel cell orientation. Thus, Liu et al. [29] take into account the vertical orientation of fuel cell flow field and subtract the gravitational pressure drop from the measured pressure drop in order to estimate the "real pressure drop". This pressure drop is expressed by:

$$\Delta P_{\mathrm{T}} = \Delta P_{\mathrm{m}} - \Delta P_{\mathrm{G}} \tag{14}$$

where ΔP_{T} is the total pressure drop in the flow field (Pa), ΔP_{m} the measured pressure drop (Pa), $\Delta P_{\mathrm{G}} = \rho g h$ the gravitational term (Pa), h the height of the water columns base at the outlet (m) and g is the gravity field (m s^{-2}).

During operation, the fuel cell may experience both flooding and drying out. Since the pressure drop variation indicates only the occurrence of a cell flooding and remains constant in case of drying [38], an efficient way to detect and distinguish the two issues is to combine the pressure drop and an adequate resistance measurement [21,38,53]. This will lead to online detection allowing corrective actions [38]. Barbir et al. [31] have dynamically recorded the pressure drop signal on a three cell stack with interdigitated channels, as well as the membrane resistance. Fig. 5 describes the evolution of different parameters in a flooded cell (pressure drop, cell voltage, resistance, stack and humidification temperatures). Experimentally, the flooding of the fuel cell was simulated by keeping the inlet gases dew point temperature higher than the cell temperature so that water condensation is favoured. The flooding was characterized by an increase in the cathodic pressure drop and by an "erratic" voltage evolution due to the sudden slug/evacuation of water. A complete recovery was observed 1500 s after the decrease of inlet gas humidification temperature. The very weak change (decrease) in resistance reflects the non-drying of the electrolyte.

In a general way, discriminating a flooding from a drying out is simple to achieve since the diagnostic tools are different for the two issues. Flooding does not affect significantly the membrane resistance nor does membrane drying out affect the pressure drop behaviour. Obviously, it is more than valuable to reinforce the combination of information and characterization methods. It is even necessary to combine the information in order to enhance the possibility and the reliability of the discrimination.

5. Conclusion

This article discusses one of the major issues impacting the PEM fuel cells durability namely, the water management. Indeed, water management impacts the PEMFC performances, stability and lifetime. The failures linked to water management can be classified in two classes which are: the flooding and the drying out, leading in the first case to concentration limitation and possibly reactant starvation and in the second case to protonic conductivity decrease. In both cases, components material degradation is noticed (mechanical degradation of the membrane, increase of the porosity, . . .). We discuss a "typical water balance" analysing the influence of each operating parameter that shows that gases flow rate and relative humidity, temperature and current density are of great influence on the water balance. On this basis, two failure trees are built, linking the causes of flooding and membrane drying out to their effects.

We also described simple characterization methods for failures linked to an improper water management, with minimum additional sensors, focussing on the "*in situ*" methods. We have demonstrated that a given defect is usually associated with several causes and a given cause can generate different consequences on the fuel cell. As a consequence, in most cases, degradation cannot be fully characterized by a single method. Therefore, a combination of two or more methods is needed to trace its origin.

Acknowledgement

The authors would like to thank the French National Research Agency (ANR), in the scope of its national action plan for hydrogen (PAN-H) for financially supporting this work.

Appendix A. Water balance

By assuming that equilibriums at both membrane/active layer interfaces are instantaneous, which implies that the water molar flow rate at the membrane side of both interfaces equals exactly the molar flow rate of water at the catalyst layer side, water molar balance in cathode, anode and membrane can, respectively, be written as follow:

$$\left(\frac{\mathrm{d}n_{\mathrm{H_2O}}}{\mathrm{d}t}\right)_{\mathrm{acc,c}} = \left(\frac{\mathrm{d}n_{\mathrm{H_2O}}}{\mathrm{d}t}\right)_{\mathrm{in,c}} - \left(\frac{\mathrm{d}n_{\mathrm{H_2O}}}{\mathrm{d}t}\right)_{\mathrm{out,c}} + \left(\frac{\mathrm{d}n_{\mathrm{H_2O}}}{\mathrm{d}t}\right)_{\mathrm{prod,c}} - \left(\frac{\mathrm{d}n_{\mathrm{H_2O}}}{\mathrm{d}t}\right)_{\mathrm{c\to m}} \tag{A.1}$$

$$\left(\frac{dn_{H_2O}}{dt}\right)_{acc,a} = \left(\frac{dn_{H_2O}}{dt}\right)_{in,a} - \left(\frac{dn_{H_2O}}{dt}\right)_{out,a} - \left(\frac{dn_{H_2O}}{dt}\right)_{a\to m} \quad (A.2)$$

$$\left(\frac{dn_{H_2O}}{dt}\right)_{acc,m} = \left(\frac{dn_{H_2O}}{dt}\right)_{c\to m} + \left(\frac{dn_{H_2O}}{dt}\right)_{a\to m} = N_{SO_3}\frac{d\lambda}{dt} = C_{SO_3}V_m\frac{d\lambda}{dt} \quad (A.3)$$

Due to the similarity between phenomena occurring at both electrodes, we can use the same equations and, in the following, the notation $(\cdot)$ will be used to describe either anode or cathode.

The water accumulation in each compartment can be split in liquid water accumulation and water vapour accumulation:

$$\left(\frac{dn_{H_2O}}{dt}\right)_{acc,(.)} = \left(\frac{dn_{H_2O}}{dt}\right)_{acc,(.),v} + \left(\frac{dn_{H_2O}}{dt}\right)_{acc,(.),l} \quad (A.4)$$

with:

$$\left(\frac{dn_{H_2O}}{dt}\right)_{acc,v} = \frac{1}{RT}\left(\frac{d}{dt}\left(V_{gas,(.)}P_{H_2O,(.)}\right)\right) = \frac{V_{T,(.)}}{RT}\left(\frac{d}{dt}\left((1-s_{(.)})P_{H_2O,(.)}\right)\right) = \frac{V_{T,(.)}}{RT}\left(\frac{dP_{H_2O,(.)}}{dt} - P_{H_2O,sat}\frac{ds_{(.)}}{dt}\right) \quad (A.5)$$

$$\left(\frac{dn_{H_2O}}{dt}\right)_{acc,(.),l} = V_{T,(.)}\cdot\frac{\rho_{H_2O,l}}{M_{H_2O}}\cdot\frac{ds_{(.)}}{dt} \quad (A.6)$$

s is the saturation or the liquid water fraction.

In Eq. (A.5), the first term at the right side corresponds to the mole variation of gaseous water in absence of liquid water and the second term corresponds to the mole variation of gaseous water in presence of liquid water. Indeed, water vapour partial pressure and volume fraction of liquid water are not strictly independent but are linked through the equilibrium between vapour and liquid water. This equilibrium implies on one hand that, if the partial pressure of water is below the saturation pressure, then liquid water cannot be present. It implies on the other hand that, if liquid water is present, then the partial pressure of vapour must equal the saturation partial pressure. As a consequence, one of the two terms at the right side of the equation is always zero, depending on the presence of liquid water.

Similarly to accumulation, all water flow rates entering and leaving the cell can be split in liquid water and water vapour flow rates. However, except very specific experimental conditions [31], water is only supplied to the cell in vapour state. As a consequence:

$$\left(\frac{dn_{H_2O}}{dt}\right)_{in,(.),v} = \frac{P_{H_2O,(.),in}}{RT}\frac{dV_{gas(.),in}}{dt} = \frac{P_{H_2O,sat}\cdot\phi_{(.),in}}{RT}\frac{dV_{gas_{(.),in}}}{dt} \quad (A.7)$$

$$\left(\frac{dn_{H_2O}}{dt}\right)_{(.),out} = \left(\frac{dn_{H_2O}}{dt}\right)_{out,(.),v} + \left(\frac{dn_{H_2O}}{dt}\right)_{out,(.),l} \quad (A.8)$$

$$\left(\frac{dn_{H_2O}}{dt}\right)_{out,(.),v} = \frac{P_{H_2O,(.),out}}{RT}\frac{dV_{gas(.),out}}{dt} = \frac{P_{H_2O,sat}\cdot\phi_{(.),out}}{RT}\frac{dV_{gas_{(.),out}}}{dt} \quad (A.9)$$

$$\left(\frac{dn_{H_2O}}{dt}\right)_{out,(.),l} = \frac{\varepsilon_{(.)}\cdot s_{(.)}\cdot\rho_l}{M_{H_2O}}v_{(.),l} \text{ [74]} \quad (A.10)$$

$$v_{(.),l} = fv_{(.),gases} - D_{(.),c}\frac{ds_{(.)}}{dx} = \frac{K_l}{\mu_l}\frac{\mu_g}{K_g}v_{(.),gases} - \frac{K_l}{\mu_l}\frac{dP_{(.)}}{ds_{(.)}}\frac{ds_{(.)}}{dx} = \frac{K_l}{\mu_l}\left(\frac{\mu_g}{K_g}v_{(.),gases} - \frac{dP_{(.)}}{dx}\right) \quad (A.11)$$

$$v_{(.),gases} = \frac{K_0}{\mu_g}(1-s_{(.)})\frac{dP_{(.)}}{dx} \text{ [74]} \quad (A.12)$$

The equation used by He et al. [74] describes the liquid flow rate in a porous media such as the GDL. In our simplified model, we do not focus on the internal molar flow rates but only on the molar flow rates entering and exiting each domain. As a consequence, we consider in Eq. (A.10), that the porosity $\varepsilon_{(.)}$ equals 1.

Combination of Eqs. (A.10)–(A.12) gives:

$$\left(\frac{dn_{H_2O}}{dt}\right)_{out,(.),l} = \frac{s_{(.)}\rho_l}{M_{H_2O}}\frac{K_l}{\mu_l}\left(\frac{K_0}{K_g}(1-s_{(.)})-1\right)\frac{dP_{(.)}}{dx} \quad (A.13)$$

For the sake of simplicity and even if we are aware that this assumption is very rough, we will assume here that, in both compartments, the total outlet gas volumetric flow rate is equal to the total inlet gas volumetric flow rate.

Taking into account the experimental results of Tang and Etzion [75] who showed that a wind flowing over a pond open to the air leaves the pond completely saturated, we will also assume that, for both compartments, the outlet gas is saturated. This assumption is reasonable since, inside a fuel cell, the atmosphere is much stuffier than over a pond in open air. This assumption also implies in our approach that the water vapour partial pressure in each compartment is constant and equals the saturation pressure.

As a consequence, taking into account these assumptions, combination of Eqs. (A.1), (A.6), (A.7), (A.9) and (A.13) leads to the following water molar balance at the cathode

compartment:

$$-P_{H_2O,sat}\frac{ds_c}{dt}\frac{V_{T,c}}{RT}+V_{T,c}\frac{\rho_{H_2O,l}}{M_{H_2O}}\frac{ds_c}{dt}$$
$$=\frac{\phi_{c,in}P_{sat}}{RT}\frac{dV_{c,in,v}}{dt}-\frac{P_{H_2O,sat}}{RT}\frac{dV_{c,v,out}}{dt}$$
$$-\frac{s_{(.)}\rho_{H_2O,l}}{M_{H_2O}}\frac{K_l}{\mu_l}\left(\frac{K_0}{K_g}(1-s_c)-1\right)(P_{cathode}-P_{atm})$$
$$+\frac{I}{2F}-\left(\frac{dn_{H_2O}}{dt}\right)_{c\to m} \quad (A.14)$$

Similarly, from combination of Eqs. (A.2), (A.6), (A.7), (A.9) and (A.13), the water molar balance at the anode compartment can be written as follow:

$$-P_{H_2O,sat}\frac{ds_a}{dt}\frac{V_{T,a}}{RT}+V_{T,a}\frac{\rho_{H_2O,l}}{M_{H_2O}}\frac{ds_a}{dt}$$
$$=\frac{\phi_{a,in}P_{sat}}{RT}\frac{dV_{a,in,v}}{dt}-\frac{P_{H_2O,sat}}{RT}\frac{dV_{a,v,out}}{dt}$$
$$-\frac{s_a\rho_{H_2O,l}}{M_{H_2O}}\frac{K_l}{\mu_l}\left(\frac{K_0}{K_g}(1-s_a)-1\right)(P_a-P_{ext})$$
$$-\left(\frac{dn_{H_2O}}{dt}\right)_{a\to m} \quad (A.15)$$

In addition, the evolution of water saturation pressure with temperature follows an exponential trend (A.16):

$$P_{H_2O,sat}=P'e^{-(M_{H_2O}h_{fg}/RT)} \quad (A.16)$$

Finally, combination of Eqs. (A.3), (A.14), (A.15) and (A.16) give, after rearrangement:

$$C_{SO_3}V_m\frac{d\lambda}{dt}+\left(\frac{\rho_{H_2O,l}}{M_{H_2O}}-\frac{P'e^{-(M_{H_2O}h_{fg}/RT)}}{RT}\right)\left(V_{T,a}\frac{ds_a}{dt}+V_{T,c}\frac{ds_c}{dt}\right)$$
$$=-\frac{P'e^{-(M_{H_2O}h_{fg}/RT)}}{RT}\left[\frac{dV_a}{dt}(1-\phi_{a,in})+\frac{dV_c}{dt}(1-\phi_{c,in})\right]$$
$$+\frac{I}{2F}-\frac{\rho_{H_2O,l}}{M_{H_2O}}\frac{K_l}{\mu_l}\left[s_a\left(\frac{K_0}{K_g}(1-s_a)-1\right)(P_a-P_{ext})\right.$$
$$\left.+s_c\left(\frac{K_0}{K_g}(1-s_c)-1\right)(P_c-P_{ext})\right] \quad (A.17)$$

This equation corresponds to equation (Eq. (10)) in the main text.

References

[1] V. Ramani, Electrochem. Soc. Interface, Spring 2006.
[2] A. Taniguchi, T. Akita, K. Yasuda, Y. Miyazaki, J. Power Sources 130 (2004) 42.
[3] X. Cheng, Z. Shi, N. Glass, L. Zhang, J. Zhang, D. Song, Z.-S. Liu, H. Wang, J. Shen, J. Power Sources 165 (2007) 739.
[4] H. Li, Y. Tang, Z. Wang, Z. Shi, S. Wu, D. Song, J. Zhang, K. Fatih, J. Zhang, H. Wang, Z. Liu, R. Abouatallah, A. Mazza, J. Power Sources 178 (2008) 103.
[5] P. Rodatz, F. Büchi, C. Onder, L. Guzzella, J. Power Sources 128 (2004) 208.
[6] G. Tian, S. Wasterlain, I. Endichi, D. Candusso, F. Harel, X. François, M.-C. Péra, D. Hissel, J.-M. Kaufmann, J. Power Sources 182 (2008) 449–461.
[7] D. Liu, Durability study of proton exchange membrane fuel cells via experimental investigations and mathematical modelling, Ph.D. thesis of the faculty of the Virginia Polytechnic Institute and State, July 11, 2006.
[8] J. Zhang, Y. Tang, C. Song, J. Zhang, H. Wang, J. Power Sources 163 (2006) 532.
[9] C. He, S. Desai, G. Brouwn, S. Bollepalli, Electrochem. Soc. Interface falls (2005).
[10] K.R. Cooper, M. Smith, J. Power Sources 160 (2006) 1088.
[11] Z. Liu, L. Yang, Z. Mao, W. Zhuge, Y. Zhang, L. Wang, J. Power Sources 157 (2006) 166.
[12] M.V. Williams, Z.H. Russell Kunz, J.M. Fenton, J. Electrochem. Soc. 152 (2005) A635.
[13] J.-M. Le Canut, A.Z. Rami, M. Abouatallah, A.D.A. Harringtonb, J. Electrochem. Soc. 153 (2006) A857.
[14] J. Larminie, A. Dicks, Fuel Cell System Explained, first ed., John Wiley & Sons, 2000.
[15] T.A. Zawodzinski Jr., C. Derouin, S. Radzinski, R.J. Sherman, T. Van, T.E. Smith, S. Springer, Gottesfeld, J. Electrochem. Soc. 140 (1993) 1041.
[16] T.A. Zawodzinski, J. Davey, R. Jestel, C. Lopez, J. Valerio, S. Gottesfeld, J. Electrochim. Acta 40 (1995) 297.
[17] A.Y. Karnic, A.G. Stefanopoulou, J. Sun, J. Power Sources 164 (2007) 590.
[18] P. Sridhar, Fuel Energy Abst. 43 (2002) 262.
[19] M. Marchand, Gestion de l'eau dans les piles à combustible, Ph.D. at the "Institut Polytechnique de Grenoble", 2005 (http://www.sudoc.abes.fr/LNG=EN/).
[20] M.A. Hickner, Cy H. Fujimoto, Chris J. Cornelius, Polymer 47 (2006) 4238.
[21] J. Stumper, M. Löhr, S. Hamada, J. Power Sources 143 (2005) 150.
[22] L. Gerbaux, Modélisation d'une pile à combustible de type hydrogène/air et validation expérimentale, Ph.D. at the "Institut National Polytechnique de Grenoble", 1996 (http://www.sudoc.abes.fr/LNG=EN/).
[23] S.D. Knights, K.M. Colbow, J. St-Pierre, D.P. Wilkinson, J. Power Sources 127 (2004) 127.
[24] T. Okada, J. Electroanal. Chem. 465 (1999) 1.
[25] D. Kramer, J. Zhang, R. Shimoi, E. Lehmann, A. Wokaun, K. Shinohara, G.G. Scherer, Electrochim. Acta 50 (2005) 2603.
[26] N. Fouquet, C. Doulet, C. Nouillant, G. Dauphin-Tanguy, B. Ould-Bouamama, J. Power Sources 159 (2006) 905.
[27] W. He, G. Lin, T.V. Ngyen, AIChE J. 49 (2003) 3221.
[28] U. Pasaogullari, C.Y. Wang, J. Electrochem. Soc. 152 (2005) A380.
[29] X. Liu, H. Guo, F. Ye, C.F. Ma, Electrochim. Acta 52 (2007) 3607.
[30] X. Liu, H. Guo, F. Ye, C.F. Ma, J. Power Sources 156 (2006) 267.
[31] F. Barbir, H. Gorgun, X. Wang, J. Power Sources 141 (2005) 96.
[32] D. Natarajan, T.V. Nguyen, AIChE J. 51 (2005) 2587.
[33] H. Meng, C.-Y. Wang, J. Electrochem. Soc. 152 (2005) A1733.
[34] H. Yamada, T. Hatanaka, H. Murata, Y. Morimoto, J. Electrochem. Soc. 153 (2006) A1748.
[35] D. Spernjak, A.K. Prasad, S.G. Advani, J. Power Sources 170 (2007) 334.
[36] J. St-Pierre, D.P. Wilkinson, S. Knights, M. Bos, J. New Mater. Electrochem. Syst. 3 (2000) 99.
[37] Handbook of Chemistry and Physics, 63rd ed., CRC Press, 1982–1983.
[38] F. Barbir, PEM Fuel Cells: Theory and Practice, Elsevier Academic Press, ISBN 012078142-3, 2005.
[39] K. Yasuda, A. Tanigushi, T. Akita, T. Ioroi, Z. Siroma, Phys. Chem. Chem. Phys 8 (2005) 746.
[40] H.P. Dhar, United States Patent 5.242.764 (February 26, 1993).
[41] F.N. Buechi, S. Srinivasan, J. Electrochem. Soc. 144 (1997) 2767.
[42] DiPierno Bosco, A. Fronk, M. Howard, United States Patent 6,103,409 (August 15, 2000).
[43] A. Hakenjos, H. Muenter, U. Wittstadt, C. Hebling, J. Power Sources 131 (2004) 213.
[44] B. Wahdame, D. Candusso, X. François, F. Harel, M.-C. Péra, D. Hissel, J.-M. Kauffmann, Int. J. Hydrogen Energy 32 (2007) 4523.
[45] D.P. Wilkinson, H.H. Voss, D.S. Watkins, B. Prater, United States Patent 005,366,818 (November 22, 1994).
[46] H.H. Voss, D.P. Wilkinson, P.G. Pickup, M.C. Johnson, V. Basura, Electrochim. Acta 40 (1995) 321.
[47] T.V. Nguyen, J. Electrochem. Soc. 143 (1996) L103.
[48] D.L. Wood, J.S. Yi, T.V. Nguyen, Electrochim. Acta 43 (1998) 3795.
[49] S. Shimpalee, U. Beuscher, J.W. Van Zee, Electrochim. Acta 52 (2007) 6748.
[50] A.P. Meyer, W. Simsbury, United States Patent 5,064,732 (November 12, 1991).
[51] B. Andreaus, A.J. McEvoy, G.G. Scherer, Electrochim. Acta 47 (2002) 2223.
[52] Yves Mortureux, Arbres de défaillance, des causes et d'évènement, Techniques de l'Ingénieur, traité CD-ROM Sécurité et gestion des risques, SE4 050 1-24.
[53] H. Görgün, M. Arcak, F. Barbir, J. Power Sources 157 (2006) 389.
[54] Ryan O'hayre, Suk-Won Cha, Whithney Clella, Fritz B. Priz, Fuel Cells Fundamentals, John Wiley & Sons, 2005, ISBN: 0-471-74148-5.
[55] J. St-Pierre, J. Electrochem. Soc. 154 (2007) B724.
[56] K. Tüber, D. Pócza, C. Hebling, J. Power Sources 124 (2003) 403.
[57] M.M. Mench, Q.L. Dong, C.Y. Wang, J. Power Sources 124 (2003) 90.
[58] H.P. Ma, H.M. Zhang, J. Hu, Y.H. Cai, B.L. Yi, J. Power Sources 162 (2006) 469.
[59] D. Hissel, M.C. Péra, J.M. Kauffmann, J. Power Sources 128 (2004) 239.
[60] D. Hissel, S. Jemeï, M.C. Péra, J.M. Kauffmann, Proceedings of the Electrimacs 2002 Conference, Montreal, Canada, 2002 (CD-ROM).
[61] D. Hissel, S. Jemeï, V. Hubert, X. François, M.C. Péra, J.M. Kauffmann, Proceedings of the 3rd International Symposium on Automotive Engineering, Gwangju, South Korea, 2001.
[62] W. Merida Donis, Diagnosis of PEMFC stack failures via electrochemical impedance spectroscopy, Ph.D. of the University of Victoria, 2002.
[63] M. Ciureanu, H. Wang, J. Electrochem. Soc. 156 (1999) 4031.
[64] T. Abe, H. Shima, K. Watanabe, Y. Ito, J. Electrochem. Soc. 151 (2004) A101.
[65] M.G. Santarelli, M.F. Torchio, P. Cochis, J. Power Sources 159 (2006) 824.
[66] T.R. Ralph, M.P. Hogarth, Platinum Metal Rev. 46 (2002) 3.
[67] Andrès Hernandez, Diagnostic d'une pile à combustible de type PEMFC, Ph.D. at the University of Technology of Belfort Montbéliard, 2006.

[68] http://www.jrc.nl/fctestnet/.
[69] C.-Y. Lim, H. R. Haas, International application published under the patent cooperation treaty (PCT), WO 2006/029254 A1, (Mar. 16, 2006).
[70] M. Smith, K. Cooper, D. Johnson, L. Scribner, Fuel Cell Mag., April–May, 2005.
[71] F. Barbir, H. Xu, H. Gorgun, Meet. Abstr. Electrochem. Soc. 501 (2006) 1522.
[72] T. Mennola, Mass transport in polymer electrolyte membrane fuel cells using natural convection for air supply, Ph.D. of the University of Technology of Helsinki, 2004.
[73] M.F. Mathias, S.A. Grot, United States Patent 6,376,111 b1 (April 23, 2002).
[74] W. He, J.S. YI, T. van Nguyen, AICHE J. 46 (2000) 2053.
[75] R. Tang, Y. Etzion, Build. Environ. 39 (2004) 77.
[76] Y. Sone, P. Ekdunge, D. Simonsson, J. Electrochem. Soc. 143 (1996) 1254.